AIP Journal of Applied Physics

Acoustic-phonon transmission and thermal conductance in a double-bend quantum waveguide

Wei-Qing Huang, Ke-Qiu Chen, Z. Shuai, Lingling Wang, Wangyu Hu, and B. S. Zou

Citation: Journal of Applied Physics **98**, 093524 (2005); doi: 10.1063/1.2127122
View online: http://dx.doi.org/10.1063/1.2127122
View Table of Contents: http://scitation.aip.org/content/aip/journal/jap/98/9?ver=pdfcov
Published by the AIP Publishing

Acoustic-phonon transmission and thermal conductance in a double-bend quantum waveguide

Wei-Qing Huang and Ke-Qiu Chen[a)]
Department of Applied Physics, Hunan University, Changsha 410082, China and Laboratory of Organic Solids, Center for Molecular Sciences, Institute of Chemistry, Chinese Academy of Sciences, Beijing 100080, China

Z. Shuai[b)]
Laboratory of Organic Solids, Center for Molecular Sciences, Institute of Chemistry, Chinese Academy of Sciences, Beijing 100080, China

Lingling Wang, Wangyu Hu, and B. S. Zou
Department of Applied Physics, Hunan University, Changsha 410082, China

(Received 17 November 2004; accepted 29 September 2005; published online 11 November 2005)

Acoustic-phonon transmission and thermal conductance in a double-bend quantum waveguide at low temperatures are investigated with the use of the scattering matrix method. The calculated results show that the total transmission coefficient versus the reduced phonon frequency exhibits a series of resonant peaks and dips. The stop-frequency gap can be observed for certain structural parameters due to the mode-mode coupling in the bend region. The universal quantum thermal conductance and the decrease of the thermal conductance at very low temperatures can be clearly observed. However, for higher temperatures where the higher transverse modes are excited, the reduced thermal conductance K/T is proportional to temperature T. The transmission coefficient and thermal conductance sensitively depend on the geometric parameters of the double bend, which provide an efficient way to control thermal conductance artificially by adjusting the parameters of the proposed microstructures. © *2005 American Institute of Physics*. [DOI: 10.1063/1.2127122]

I. INTRODUCTION

In recent years, the heat transport by phonons in mesoscopic systems have attracted much attention.[1,2] Up to date, many intriguing investigations of diffusive phonon transport in various kinds of nanostructures, such as thin film,[3–6] quantum well,[7] superlattices,[8–11] nanowires,[12–17] one-dimensional glass,[18] and nanotube[19] have been reported. At the same time, increasing attention is also paid to elucidate ballistic phonon heat transport in mesoscopic systems. Following Landauer's approach to electronic conductance, several groups[20–24] have derived expressions of thermal conductance for ballistic phonon transport at low enough temperatures in an ideal elastic beam and found that the thermal conductance at low temperatures is dominated by the lowest modes with zero cutoff frequency and takes a universal value $k_{ph} = \pi^2 k_B^2 T/3h$, analogous to the well-known $2e^2/h$ electronic conductance quantum. These predictions have been verified by experiment.[25] More recently, the phonon transmission and thermal conductance in the quantum waveguide structures[26–28] have been investigated using the scattering matrix method. Some interesting features are revealed, such as acoustic -phonon mode splitting behavior and the noninteger quantized thermal conductance in an asymmetric y-branch three-terminal junction,[28] and phonon transmission and thermal conductance can be controlled by adjusting the parameters of the stub in a T-shaped waveguide structure.[27]

Motivated by these works, in this paper we investigate the phonon transmission and thermal conductance in a double-bend quantum waveguide structure, schematically shown in Fig. 1. The properties of electron transport in the same structure have been studied experimentally[29] and theoretically.[30,31] It was found that the transmission coefficient shows strong resonance effects due to the presence of a perpendicular single right-angle bend. It was also found that in such a structure the stop-band behavior appears, at which all electrons are reflected by the double bend. The present paper is to calculate the phonon transmission and thermal conductance in such a system by using scattering matrix,[32–34] which is an effective method to calculate the electronic or phonon transport in one-dimensional or quasi-one- dimensional mesoscopic systems. Our results show some interesting physical properties such as periodic transmission spectra,

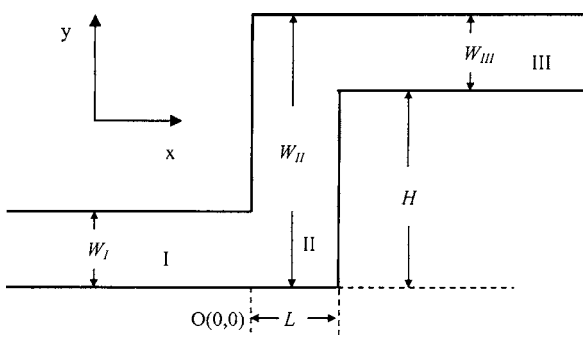

FIG. 1. Schematic illustration of the double-bend quantum waveguide structure.

[a)]Author to whom correspondence should be addressed; electronic mail: keqiuchen@iccas.ac.cn or keqiuchen@hnu.cn (K.-Q. Chen)
[b)]Electronic mail: zgshuai@iccas.ac.cn (Z. Shuai)

stop-frequency gap, resonant peak-dip structures, the universal quantum thermal conductance, and so on.

This paper is organized as follows. In Sec. II, a brief description of the model and the necessary formulas used in the calculations is given. The numerical results are presented in Sec. III with analyses. Finally, we summarize our results in Sec. IV.

II. MODEL AND FORMALISM

The model structure shown in Fig. 1 is divided into three regions, i.e., region I for $x<0$, region II for $0<x<L$, and region III for $x>L$. The transverse dimension of the three regions are for W_{I}, W_{II}, and W_{III}, respectively. We denote the width and height of the bend as L and H, respectively. It is assumed that the temperatures in regions I and III are T_1 and T_3, respectively, and the difference δT $(\delta T=T_1-T_3>0)$ is very small. So we can adopt the mean temperature $T[T=(T_1=(T_1+T_3)/2)]$ as the temperature of regions I and III in the following calculations. For the quantum structure depicted in Fig. 1, there exist three types of acoustic modes: longitudinal polarized P mode, vertically polarized SV mode and horizontally polarized shear SH mode, as expounded by Graff.[35] Their polarization directions are along the x, y, and z directions, respectively. When P mode transports into the waveguide, the reflection at the interfaces may lead to the mode conversion, namely, its reflection wave and the transmission wave may contain both P and SV modes. The situation is similar to the SV mode incidence. Then the mixing of P and SV modes would occur. However, considering our assumption that regions I, II, and III have the same thickness and are small with respect to the other dimensions and also to the wavelength of the elastic waves, the horizontally polarized shear SH mode is decoupled from the P or SV mode polarized in the x-y plane. Our previous work investigated the effect of mode mixing between SV and P modes on the thermal conductance at low enough temperatures in a T-type structure.[27] The results show that at a low temperature, the effect of mode mixing on the thermal conductance is very small, and that the thermal conductance of the SH wave has similar features to those of the P (or SV) mode. Taking into account the fact that the present work focuses on the quantized effects on the acoustic -phonon thermal transport features at low enough temperatures, so we only discuss the SH mode.

Considering imperfect contact at the regions I and III the thermal conductance K takes the form[20,23]

$$K=\frac{\hbar^2}{k_B T^2}\sum_m \frac{1}{2\pi}\int_{\omega_m}^{\infty}\tau_m(\omega)\frac{\omega^2 e^{\beta\hbar\omega}}{(e^{\beta\hbar\omega}-1)^2}d\omega. \tag{1}$$

Here $\tau_m(\omega)$ is the transmission coefficient from mode m of region I at frequency ω across all the interfaces into the modes of region III; ω_m is the cutoff frequency of the mth mode, $\beta=1/(k_B T)$, k_B is the Boltzman constant, T is the temperature, and $\hbar$ is Planck's constant. The effect of scattering is introduced through the transmission coefficient $\tau_m(\omega)$. $\tau_m(\omega)<1$ corresponds to a reduction in the transport due to the scattering by bend region. Thus, the essential issue in predicting the thermal conductance is to calculate the transmission coefficient $\tau_m(\omega)$.

In this paper, we employ the elastic model to calculate the transmission coefficient of acoustic phonon. Our work focuses on SH mode propagating in the z direction. In the elastic approximation, the displacement fields of the decoupled SH mode is governed by a single scalar equation:

$$\nabla^2\psi=\frac{1}{c^2}\frac{\partial^2\psi}{\partial t^2}, \tag{2}$$

where the SH wave velocity v_{SH} is related to the mass density ρ and elastic stiffness constant C_{44},

$$v_{\mathrm{SH}}=\sqrt{C_{44}/\rho}. \tag{3}$$

According to the stress-free boundary condition at edges,

$$\hat{n}\cdot\nabla\psi=0, \tag{4}$$

where $\hat{n}$ is normal to the edge, the phonon displacement field equations in the three regions (denoted as ψ^{I}, ψ^{II}, and ψ^{III}) can be expressed as

$$\psi^{\mathrm{I}}(x,y)=\sum_{n=1}^{N^{\mathrm{I}}}[C_n^{\mathrm{I}}e^{ik_n^{\mathrm{I}}x}+D_n^{\mathrm{I}}e^{-ik_n^{\mathrm{I}}x}]\phi_n^{\mathrm{I}}(y), \tag{5}$$

$$\psi^{\mathrm{II}}(x,y)=\sum_{n=1}^{N^{\mathrm{II}}}[C_n^{\mathrm{II}}e^{ik_n^{\mathrm{II}}x}+D_n^{\mathrm{II}}e^{-ik_n^{\mathrm{II}}x}]\phi_n^{\mathrm{II}}(y), \tag{6}$$

and

$$\psi^{\mathrm{III}}(x,y)=\sum_{n=1}^{N^{\mathrm{III}}}[C_n^{\mathrm{III}}e^{ik_n^{\mathrm{III}}(x-L)}+D_n^{\mathrm{III}}e^{-ik_n^{\mathrm{III}}(x-L)}]\phi_n^{\mathrm{III}}(y), \tag{7}$$

where C_n^{ξ} and D_n^{ξ} $[\xi$: I, II, and III$]$ are constants to be determined by matching the boundary conditions. $\phi_n^{\xi}(y)$ represents the orthogonal transverse mode n in region ξ,

$$\phi_n^{\xi}(y)=\begin{cases}\sqrt{\dfrac{2}{W_\xi}}\cos\dfrac{n\pi}{W_\xi}y & (n\neq 0)\\ \sqrt{\dfrac{1}{W_\xi}} & (n=0);\end{cases} \tag{8}$$

k_n^{ξ} can be expressed in terms of incident phonon frequency ω, the SH wave velocity v_{SH}^{ξ}, and the transverse dimension ω_ξ of region ξ by the energy conservation condition:

$$\omega^2=(k_n^{\xi})^2(v_{\mathrm{SH}}^{\xi})^2+\frac{n^2\pi^2(v_{\mathrm{SH}}^{\xi})^2}{w_\xi^2}. \tag{9}$$

In principle, the sum over n in Eqs. (5)–(7) includes all propagating modes and evanescent modes (imaginary k_n^{ξ}). However, in the real calculations, we take all the propagating modes and several lowest evanescent modes into account to meet the desired precision. The matching conditions are determined by the requirement of continuity of the displacement ψ and the stress $C_{44}\partial\psi/\partial x$ at the interfaces I-II and II-III,

$$\psi^{\mathrm{I}}(x=0,y)=\psi^{\mathrm{II}}(x=0,y), \tag{10}$$

$$[\partial\psi^{\mathrm{I}}(x,y)/\partial x]|_{x=0}=[\partial\psi^{\mathrm{II}}(x,y)/\partial x]|_{x=0}, \tag{11}$$

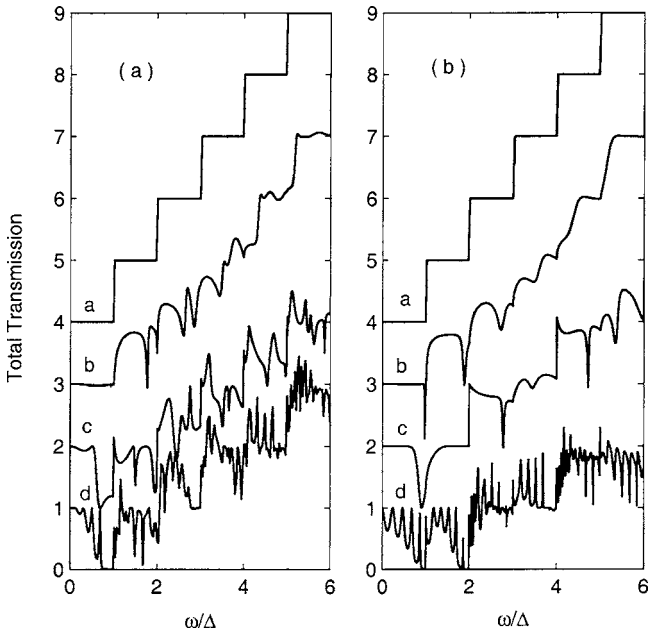

FIG. 2. Total transmission coefficient as a function of the reduced frequency ω/Δ of the incident phonons for the double-bend acoustic waveguide structure: (a) and (b) correspond to the width $L=12$ and 6 nm, respectively. Curves *a*, *b*, *c*, and *d* correspond to the height $H=0$, 2, 12, and 60 nm in (a) and $H=0$, 2, 6, and 60 nm in (b), respectively. Here, we take $W_{\mathrm{I}}=W_{\mathrm{III}}=12$ nm. Two consecutive curves are vertically offset for clarity.

$$\psi^{\mathrm{II}}(x=L,y)=\psi^{\mathrm{III}}(x=L,y), \tag{12}$$

$$[\partial\psi^{\mathrm{II}}(x,y)/\partial x]|_{x=L}=[\partial\psi^{\mathrm{III}}(x,y)/\partial x]|_{x=L}. \tag{13}$$

Multiplying Eq. (10) by $\phi_n^{\mathrm{I}}(y)$, Eqs. (11) and (12) by $\phi_n^{\mathrm{II}}(y)$, and Eq. (13) by $\phi_n^{\mathrm{III}}(y)$, respectively, and then integrating over y, we obtain the equations for the coefficients in Eqs. (5)–(7) required. After rewriting the equations in the form of a matrix, we can derive the transmission coefficient τ_m by the scattering matrix method.[32–34]

In the following numerical calculations, we employ the following values of elastic stiffness constant and the mass density:[36] $C_{44}(\mathrm{GaAs})=5.99$ $(10^{10}$ N m$^{-2})$ and $\rho(\mathrm{GaAs})=5317.6$ (kg m^{-3}).

III. NUMERICAL RESULTS AND DISCUSSION

Figure 2 displays the dependence of the total transmission coefficients on the reduced frequency ω/Δ for different bend heights H in the structure, as depicted in Fig. 1. Here, $\Delta=\omega_{n+1}-\omega_n=\pi v_{\mathrm{SH}}/W_{\mathrm{I}}$ (v_{SH} is the acoustic wave velocity in region I) denotes the splitting of the cutoff frequency between the $(n+1)$th and nth modes in region I. Hereafter, we always choose $W_{\mathrm{I}}=W_{\mathrm{III}}=12$ nm in the calculations. When the bend is absent, namely, the structure is recovered to a straight quantum waveguide, curve *a* in Fig. 2 shows smooth transmission steps and an abrupt jump is always located just at an integer-reduced frequency, where a new mode starts to be excited. These perfect steps show that in such a case there is no imperfect coupling and ballistic transport through the structure occurs, which are similar to the electronic transmission in a similar structure.[29] However, it is clearly seen from Fig. 2 that when $\omega\to 0$ the phonon transmission approaches unity, unlike the case of electrical transport, where the transmission is always close to zero when the energy of the incident electron $\varepsilon_F<\varepsilon_1$ (ε_1 is the threshold energy of the lowest mode). This results from the stress-free boundary condition which allows the propagation of the acoustic mode with $\omega\to 0$, which has also been discussed in detail in Ref. 26. When H is increased to 2 nm, the transmission plateaus are observed to resolve into a number of peak-dip structures, except the first plateaus being almost unchanged. With further increase of the height H, the transmission spectrum display more complex oscillation behaviors [see curves *c* and *d* in Fig. 2(a)], and the lowest plateaus are also destroyed. Similar behaviors of the ballistic electron transmission have also been found in the same structure.[29–31] These phenomena can be well understood. Increasing the height of the bend H leads to a lowering of the cutoff frequency of the propagating wave along the bend. Thus, more modes can be excited in the bend when the height of the bend H is higher. These modes will interfere with each other due to the multiple reflection of the phonon waves in the bend region. In general, the more modes interfere with each other in the bend region, the more complex are the transmission spectra, especially for higher frequency. Figure 2(a) also shows that the total transmission coefficients decrease with the increasing height H except the lowest plateaus, and the change in the higher frequency is faster than that of the lower one. The reason is that the reflection of the phonons becomes stronger as the height H is increased. Comparing Fig. 2(a) with 2(b), we can find that the transmission coefficients become smaller when the width L is decreased, especially for large H. This can be well understood. The smaller the width L, the stronger the reflection of the phonons due to the bend. Consequently, the transmission coefficient decreases. An interesting feature in Fig. 2 is that a dip is always located just before the opening of a new mode. These dips broaden with the increase of the height of the bend and some of them gradually develop into stop-frequency gaps, at which all phonons are reflected by the double-bend structure. By further calculations, it is found that the stop-frequency behavior occurs only when $H\geqslant L$, and only a stop-frequency gap appears when $L\geqslant W_{\mathrm{I}}$, while two stop-frequency gaps can be observed when $L<W_{\mathrm{I}}$ for large H. The appearance of dip or stop-frequency gap originates from the coupling between the incident mode and the reflection mode of the bend. With the increase of the height of the bend, the coupling becomes stronger between the incident modes and reflection modes due to the increasing of the strength of the phonon reflections. The stronger the coupling, the broader the width of the dip or stop-frequency gap. These results may be useful for the design of phonon devices.

To more clearly reveal the transmission properties of mode 0, we show the transmission coefficient dependence on the the height H and the incident phonon frequency ω/Δ for mode 0 in the system, as shown in Fig. 3. As can be seen, the transmission coefficients always approach unity as $\omega\to 0$, indicating that the transmission is independent on the bend for incident acoustic phonon with $\omega\to 0$. This is actually anticipated since at $\omega\to 0$, the wavelength of the phonon is very large and much larger than the dimension of the scat-

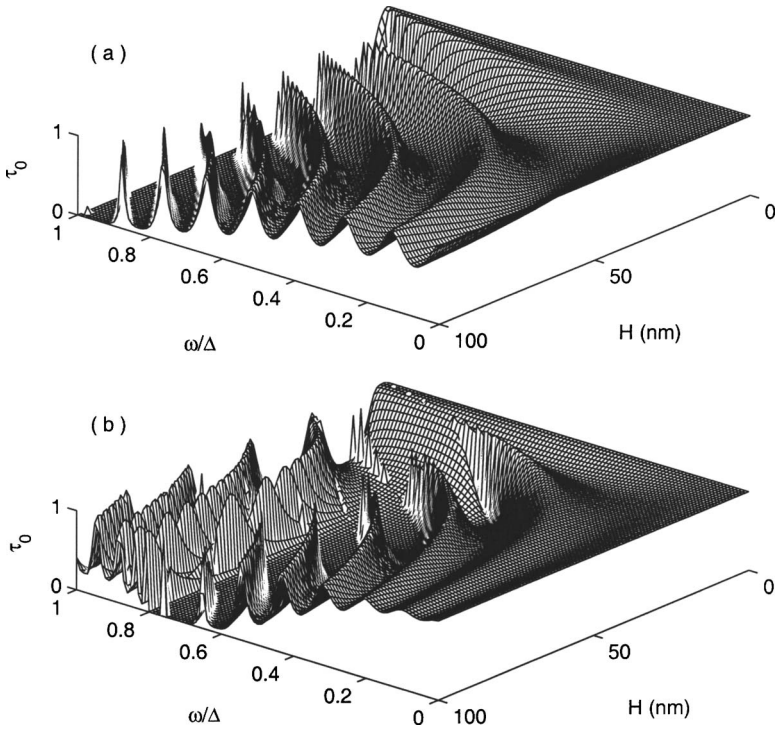

FIG. 3. Transmission coefficient vs the height H and the incident phonon frequency ω/Δ for a double-bend acoustic waveguide structure with $W_{\mathrm{I}}=W_{\mathrm{III}}=12$ nm, where $\Delta=\omega_{n+1}-\omega_n=\pi v_{\mathrm{SH}}/W_{\mathrm{I}}$ (v_{SH} is the acoustic wave velocity in GaAs) represents the splitting of the cutoff frequency between the $(n+1)$th mode and the nth mode in region I. (a) for $L=6$ nm; (b) for $L=15$ nm.

tering region (i.e., L and W_{II}); the displacement field ψ becomes essentially the same throughout. From Fig. 3(a), it can be seen that when $L=6$ nm the transmission exhibits a periodic pattern as a function of H when $0<\omega/\Delta<1.0$. The oscillation period ΔH can be obtain from $2k_{\mathrm{SH}}\Delta H=2\pi$, where $k_{\mathrm{SH}}=\sqrt{\omega^2/v_{\mathrm{SH}}^2}$ is the wave vector of phonon propagating along the y direction in region II. For $L=15$ nm, as shown in Fig. 3(b), the periodic pattern of the transmission coefficient is destroyed when $\omega/\Delta>0.7$. These results and further calculations indicate that the range of the frequency which the transmission exhibits a periodic pattern becomes smaller as the width of the bend is increased when $L>12$ nm.

To further elucidate the dependence of the transmission coefficients on the bend height H and the width L, the transmission coefficient of the lowest mode with transversal index $n=0$ as a function of H for different L and different frequencies are depicted in Fig. 4: (a)–(d) correspond to $L=6$, 12, 15, and 24 nm, respectively. It is clearly seen from the figure that changing H or L can cause significant changes in the transmission for given frequencies. We first consider the case $\omega/\Delta=1.0$. The transmission coefficients show some interesting features: (1) When $L\leqslant 12$ nm, the transmission coefficient decreases rapidly from unity to zero as H is increased. And the smaller the width L, the faster the decrease of the transmission coefficient; (2) When $12<L<24$ nm, the transmission coefficients exhibit a periodic oscillation. By calculations, it is found that the period is decreased with the increase of L; (3) when $L\geqslant 24$ nm, the transmission spectra exhibit a series of nonregular peak-dip structures. By comparing the transmission spectra with different ω/Δ, it can be found that the transmission coefficients and oscillation period are strongly dependent on the incident phonon frequency, the width L, and the height H.

We now turn to discuss the effect of the structural parameters on the thermal conductance. Figure 5 shows the thermal conductance divided by temperature reduced by the zero-temperature universal $\pi^2k_B^2/3h$ as a function of the reduced temperature $k_BT/\hbar\Delta_{\mathrm{SH}}$ for different heights H. Figure 5(a) is for the total conductance and Figs. 5(b)–5(d) correspond to the reduced thermal conductance of modes 0, 1, and

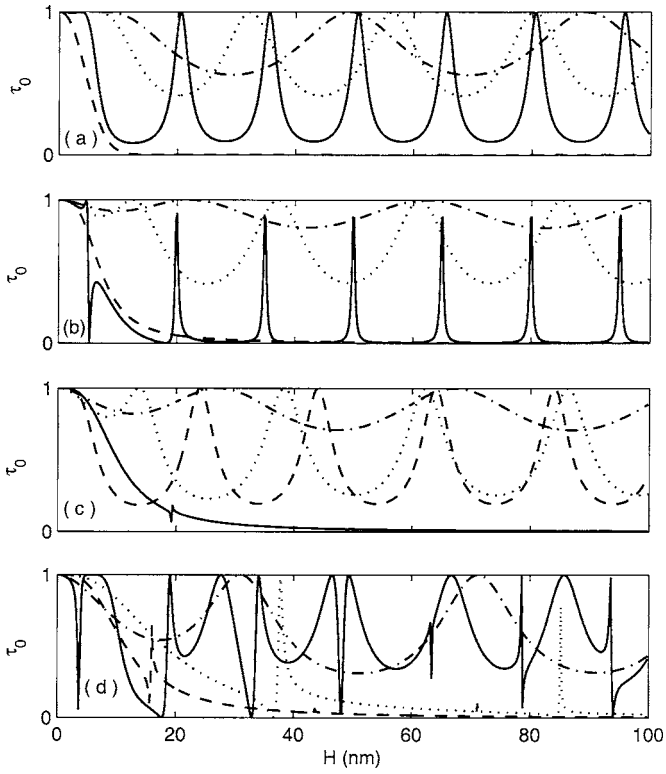

FIG. 4. Transmission coefficient as a function of the height H for different frequencies: (a)–(d) correspond to $L=6$, 12, 15, and 24 nm, respectively. The dash-dotted, dotted, solid, and dashed curves are for $\omega/\Delta=0.3$, 0.5, 0.8, and 1.0, respectively. Here we take $H=12$ nm.

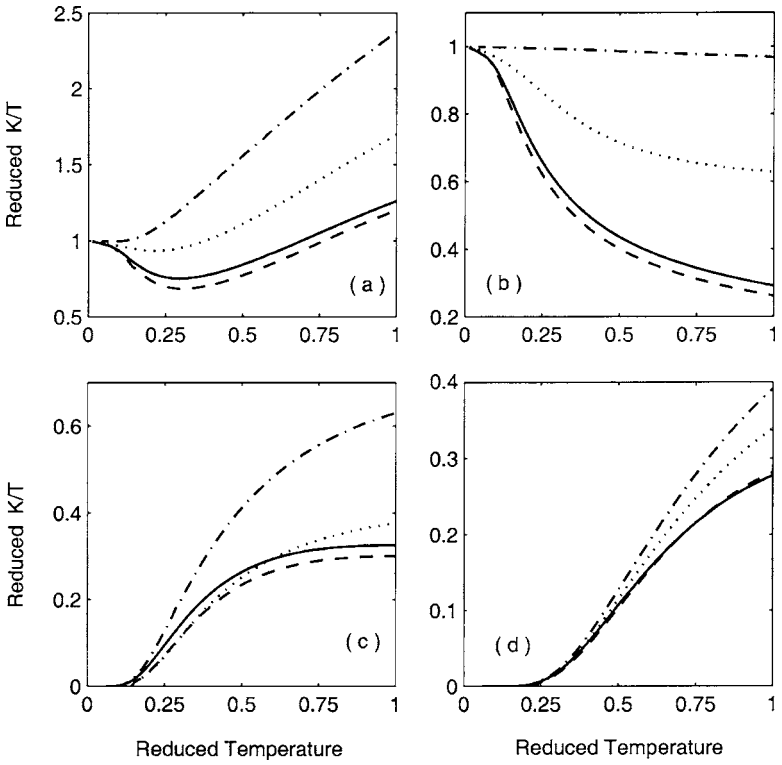

FIG. 5. Thermal conductance divided by temperature reduced by the zero-temperature universal value $\pi^2 k_B^2/3h$ as a function of the reduced temperature $k_B T/\hbar\Delta$ for the different heights H. (a) is for the total thermal conductance and (b)–(d) for the thermal conductance of modes 0, 1, and 2, respectively. The dash-dotted, dotted, solid, and dashed curves correspond to $H=1$, 5, 12, and 15 nm, respectively. Here we take $L=12$ nm.

2, respectively. It should be pointed out that the total conductance is the summation of the thermal conductance of the first six modes. It can be clearly seen from Fig. 5(a) that as the temperature $T\rightarrow 0$ where only the transverse mode $m=0$ can be excited, the value of thermal conductance K/T approaches the ideal universal value $\pi^2 k_B^2/3h$ and it is independent on the geometry of the structure. This indicates that the scattering of the bend on the long-wavelength acoustic waves with $\omega\rightarrow 0$ and wave vector $k\rightarrow 0$ is very small. For the structure with $H=1$ nm, a thermal conductance plateau appears under low temperatures due to the height of the bend being far smaller than the width of the main wire and so the scattering by the bend is very small. With an increase of temperature T, the plateau terminates and the value of K/T linearly increases. This is because the higher transverse modes $m(m>0)$ are excited and contribute to the thermal conductance at higher temperatures [as shown in Figs. 5(c) and 5(d)]. This accords with the fact that at a higher temperature the energy contributed by each mode is given by classical equipartition and the two-dimensional heat cavity is proportional to T^2, and so the value of $K/T\propto T$. It is also obvious that with an increase of the height H the reduced thermal conductance K/T shifts down and the thermal conductance plateau disappears, and the change is more sensitive to the smaller H. Further calculations show that when $H>18$ nm the reduced thermal conductance was kept almost unchanged. From Fig. 5(b), it is clearly seen that the reduced thermal conductance of mode 0 is decreased with the increase of temperature. This can be attributed to the resonance coupling between the zero mode in the main wire and the zero mode in the bend region, which leads to the lower transmission coefficient under the given parameters. It is also evidently seen that when $H<12$ nm the reduction of the reduced thermal conductance K/T is very sensitive to the change of the height H. However, further increasing H, the change of K/T of mode 0 is very small. On the contrary, the reduced thermal conductance of the higher modes (i.e., $m=1,2,3,\ldots$) increases with temperature. It can also be seen from Figs. 5(b)–5(d) that the reduced thermal conductance K/T decreases with the increase of the index m. By calculation it is found that the reduced thermal conductance of mode 6 is very small for the explored temperature range. Therefore only the first six modes can make their contributions to the total thermal conductance for the explored temperature scope. From Fig. 5(b), it is clearly seen that with the increase of the height H, the value K/T of the zero mode decreases monotonically. However, we can find from Fig. 5(c) that the value K/T of mode 1 at $H=12$ nm is bigger than that at $H=5$ nm for the certain temperature range. Similar phenomena can also be found for mode 2 in Fig. 5(d). In general, the bigger the height H, the stronger the scattering of the bend on the phonon modes and the smaller the value K/T. However, the reverse cases may occur due to the different coupling strengths between the incident modes and the scattering modes for different indexes of the modes and temperature.

We now envisage the influence of the bend width L on the thermal conductance. The calculated total thermal conductance as a function of reduced temperature are depicted in Fig. 6(a) for different widths L at $H=12$ nm. It is clear that the total thermal conductance presents a strong dependence on the bend width L: The total reduced thermal conductance decreases rapidly firstly from unity, then increases with the increase of the reduced temperature, and the change with smaller width is faster than that with a larger one. However, when the width $L>12$ nm (i.e., $L>W_I$), a reverse case occurs where the reduced thermal conductance is decreased with the increase of L at lower temperature ($T<0.3$). In or-

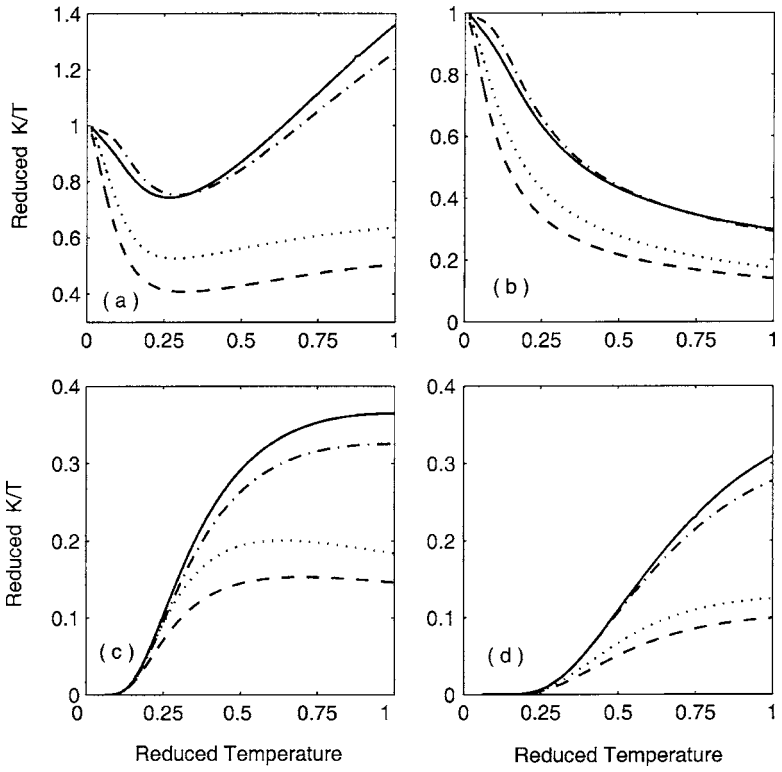

FIG. 6. Thermal conductance divided by temperature reduced by the zero-temperature universal value $\pi^2 k_B^2/3h$ as a function of the reduced temperature $k_B T/\hbar\Delta$ for the different widths L. (a) is for the total thermal conductance and (b)–(d) for the thermal conductance of modes 0, 1, and 2, respectively. The dashed, dotted, dash-dotted, and solid curves correspond to $L=1$, 2, 12, and 15 nm, respectively. Here we take $H=12$ nm.

der to explore these phenomena, we also present the reduced thermal conductance of individual modes in Figs. 6(b)–6(d). From Fig. 6(b), we can see that the reduced thermal conductance of mode 0 increases with the width L when $L \leqslant 12$ nm. However, when $L > 12$ nm, the reduced thermal conductance decreases with an increase of L at lower temperature (<0.7). From Figs. 6(c) and 6(d), it is clearly seen that the conductances of modes 1 and 2 increase slowly as the width L is increased. It is the combination of the three modes that leads to the behaviors of the total K/T due to it being contributed mainly by the first three modes, especially mode 0. According to the results presented above, we can control the heat conductance to a certain degree by adjusting the structural parameters, which may be important for application in devices.

IV. SUMMARY

In this paper, we have presented a numerical calculation of the phonon transmission and thermal conductance in the double-bend quantum waveguide at low temperatures. Some interesting features are observed. The total transmission coefficient versus the reduced frequency exhibits a series of resonant peaks and dips. When the height is larger than the width of the bend, the stop-frequency gap appears, at which all phonons are reflected by the double bend. The stress-free boundary condition of an acoustic phonon leads to the propagation of the zero mode. When only the zero mode is excited in the bend region, the transmission spectra will vary periodically with the height of the bend. However, when more than one mode are excited, the periodicity will be destroyed due to the mode-mode coupling in the bend region. The total thermal conductance reaches the universal quantum thermal conductance at zero temperature, and then decreases with the increase of the temperature. For higher temperatures where the higher transverse modes start to contribute to the thermal conductance, the thermal conductance behaves as $K/T \propto T$. The calculated results show that the total thermal conductance is also very sensitive to the height and width of the bend. It is expected that by adjusting the structural parameters one can control the transmission spectrum and thermal conductance of the proposed structure to match practical requirements in devices.

ACKNOWLEDGMENTS

This work was supported by the National Natural Science Foundation of China and the Chinese Academy of Science.

[1] G. Chen, Int. J. Therm. Sci. **39**, 471 (2000); Phys. Rev. Lett. **86**, 2297 (2001).
[2] D. G. Cahill, W. K. Ford, K. E. Goodson, G. D. Mahan, A. Majumdar, H. J. Maris, R. Merlin, and S. R. Phillpot, J. Appl. Phys. **93**, 793 (2003).
[3] Y. S. Ju and K. E. Goodson, Appl. Phys. Lett. **74**, 3005 (1999).
[4] W. Liu and M. Asheghi, Appl. Phys. Lett. **84**, 3819 (2004).
[5] D. Song and G. Chen, Appl. Phys. Lett. **84**, 687 (2004).
[6] D. Song, W.-N. Shen, B. Dunn, C. D. Moore, M. S. Goorsky, T. Radetic, R. Gronsky, and G. Chen, Appl. Phys. Lett. **84**, 1883 (2004).
[7] A. Balandin and K. L. Wang, Phys. Rev. B **58**, 1544 (1998).
[8] S. M. Lee, D. G. Cahill, and R. Venkatasubramanian, Appl. Phys. Lett. **70**, 2957 (1997).
[9] G. Chen and M. Neagu, Appl. Phys. Lett. **71**, 2761 (1997).
[10] M. V. Simkin and G. D. Mahan, Phys. Rev. Lett. **84**, 927 (2000).
[11] S. T. Huxtable *et al.*, Appl. Phys. Lett. **80**, 1737 (2002).
[12] S. G. Volz and G. Chen, Appl. Phys. Lett. **75**, 2056 (1999).
[13] B. A. Glavin, Phys. Rev. Lett. **86**, 4318 (2001).
[14] J. Zou and A. Balandin, J. Appl. Phys. **89**, 2932 (2001).
[15] X. Lü, J. H. Chu, and W. Z. Shen, J. Appl. Phys. **93**, 1219 (2003).
[16] D. Y. Li, Y. Wu, P. Kim, L. Shi, P. Yang, and A. Majumdar, Appl. Phys. Lett. **83**, 2934 (2003).
[17] N. Mingo, L. Yang, D. Y. Li, and A. Majumdar, Nano Lett. **3**, 1713 (2003); N. Mingo, Phys. Rev. B **68**, 113308 (2003).

[18]D. M. Leitner, Phys. Rev. B **64**, 094201 (2001).
[19]P. Kim, L. Shi, A. Majumdar, and P. L. McEuen, Phys. Rev. Lett. **87**, 215502 (2001).
[20]L. G. C. Rego and G. Kirczenow, Phys. Rev. Lett. **81**, 232 (1998).
[21]D. E. Angelescu, M. C. Cross, and M. L. Roukes, Superlattices Microstruct. **23**, 673 (1998).
[22]M. P. Blencowe, Phys. Rev. B **59**, 4992 (1999).
[23]M. C. Cross and R. Lifshitz, Phys. Rev. B **64**, 085324 (2001).
[24]D. H. Santamore and M. C. Cross, Phys. Rev. Lett. **87**, 115502 (2001); Phys. Rev. B **63**, 184306 (2001).
[25]K. Schwab, E. A. Henriksen, J. M. Worlock, and M. L. Roukes, Nature (London) **404**, 974 (2000).
[26]W.-X. Li, K.-Q. Chen, W. H. Duan, J. Wu, and B. L. Gu, J. Phys. D **36**, 3027 (2003).
[27]W.-X. Li, K.-Q. Chen, W. H. Duan, J. Wu, and B. L. Gu, J. Phys.: Condens. Matter **16**, 5049 (2004).
[28]W.-X. Li, K.-Q. Chen, W. H. Duan, J. Wu, and B. L. Gu, Appl. Phys. Lett. **85**, 822 (2004).
[29]J. C. Wu and M. N. Wybourne, Appl. Phys. Lett. **59**, 102 (1991).
[30]A. Weisshaar, J. Lary, S. M. Goodnick, and V. K. Tripathi, Appl. Phys. Lett. **55**, 2114 (1989).
[31]A. Weisshaar, J. Lary, S. M. Goodnick, and V. K. Tripathi, J. Appl. Phys. **70**, 355 (1991).
[32]H. Tamura and T. Ando, Phys. Rev. B **44**, 1792 (1991).
[33]M. Leng and C. S. Lent, Phys. Rev. Lett. **71**, 137 (1993); Phys. Rev. B **50**, 10823 (1994).
[34]H. Q. Xu, Phys. Rev. B **52**, 5803 (1995); Appl. Phys. Lett. **80**, 853 (2002).
[35]K. F. Graff, *Wave Motion in Elastic Solids* (Clarendon, Oxford, 1975).
[36]O. Madelung, *Semiconductors: Group IV Elements and III-V Compounds* (Springer, Berlin, 1982).